International Journal of Veterinary Science and Medicine 6 (2018) 286–295

HOSTED BY

Contents lists available at ScienceDirect

International Journal of Veterinary Science and Medicine

journal homepage: www.elsevier.com/locate/ijvsm

Full Length Article

Microwave assisted green synthesis of Hydroxyapatite nanorods using *Moringa oleifera* flower extract and its antimicrobial applications

V. Kalaiselvi[a,b,*], R. Mathammal[a], S. Vijayakumar[c], B. Vaseeharan[c]

[a] Department of Physics, Sri Sarada College for Women, Salem - 636 016, Tamil Nadu, India
[b] Department of Physics, Navarasam Arts & Science College for Women, Arachalur, Erode- 638101, Tamil Nadu, India
[c] Nanobiosciences and Nanopharmacology Division, Biomaterials and Biotechnology in Animal Health Lab, Department of Animal Health and Management, Alagappa University, Science Campus 6th Floor, Karaikudi 630 004, Tamil Nadu, India

ARTICLE INFO

Keywords:
Antibacterial
Antifungal, *Candida albicans*
Aspergillus fumigatus
Hydroxyapatite
Moringa flower

ABSTRACT

Hydroxyapatite is an important biomaterial and main mineral component found in bones for potential clinical applications. *Moringa oleifera,* a common plant in which all parts are edible and rich in iron content. This study reported the chemically synthesized Hydroxyapatite and green synthesis of Hydroxyapatite nanorods using the aqueous flower extract of *Moringa oleifera* by microwave assisted method. The synthesized *Moringa oleifera* flower extract Hydroxyapatite nanorods were characterized by UV–Vis spectroscopy (UV–vis), Fourier Transform Infra Red spectroscopy (FTIR), X-Ray Diffraction analysis (XRD), Transmission Electron Microscopy (TEM), Photo Luminescence spectroscopy (PL), Thermo Gravimetric analysis (TGA) and Energy Dispersive X-ray analysis (EDX). In addition, the antimicrobial activity of these nanorods was assessed. *Moringa oleifera* flower extract Hydroxyapatite nanorods were crystalline in nature, rod like structure with a mean particle size of 41 nm. The antibacterial activity of *Moringa oleifera* flower extract capped Hydroxyapatite nanorods was greater against Gram positive bacteria than Gram negative bacteria. Furthermore, *Moringa oleifera* extract capped Hydroxyapatite nanorods showed a very good antifungal activity against three common pathogenic fungi including; *Candida albicans*, *Aspergillus fumigatus* and *Aspergillus niger*.

1. Introduction

In recent years, applications of nanomaterials are getting more generalized covering different fields including optoelectronics, catalysis, Biomedical and sensor devices among the bulk materials. Parameters like structure, size and elemental composition are important besides the quantum size effects in materials for nanometer scale for their promising applications. The bone substitutes should be prepared for individual patients with all details controlled on the micrometer level [1]. The main mineral constituent of bone is calcium. Hence calcium orthophosphate acts as a main component in biological systems. Hydroxyapatite, the main source of calcium, is substituted in the field of dentistry, prosthetic applications, bone tissue engineering, orthopedic and dental implant coating. The stoichiometric ratio of Hydroxyapatite was calcium and phosphorous in the ratio of 1:67, which resembles the human bone [2,3]. The biocompatible targeted drug delivery systems, controlling the rate and time period of the drug delivery and simultaneously eliminating toxic and side effects on the healthy tissues, are of great interest.

Extensive attempts have been made to develop a simple, efficient and green synthesis method to form biofunctional and implant coatings possessing a significant biocompatibility, a bioactivity and a mechanical strength. Hydroxyapatite, as a major mineral component of vertebrate bones and teeth, is an excellent material for drug delivery [4,5]. The plant extract facilitated green synthesis has gained a wide attention and emerged as an active research area in the field of nanotechnology. Plant extracts consisted of tannins and polyphenol are widely applied in food processing as natural additives to edible foods and in leather industry for fabrication. The polyphenolic OH groups have good affinity towards metal ions; hence the plant extract is widely applied as a reducing, stabilizing and chelating agent [6,7]. *Moringa oleifera* flower (MOF) is also known as drumstick and horse radish. All parts of the MOF are nutrient rich and edible, also seeds are used in biodiesel extraction. It has good antioxidant property due to the presence of excess polyphenol, alkaloids, tannins, flavonoids, vitamins, minerals and carotenoids. Due to rich tannins in MOF, it is widely applied in green

Peer review under responsibility of Faculty of Veterinary Medicine, Cairo University.
* Corresponding author. at: Department of Physics, Navarasam Arts & Science College for Women, Arachalur, Erode - 638101, Tamil Nadu, India.
E-mail address: nk.arthi.kalai@gmail.com (V. Kalaiselvi).

https://doi.org/10.1016/j.ijvsm.2018.08.003
Received 11 June 2018; Received in revised form 13 August 2018; Accepted 13 August 2018
Available online 30 August 2018

synthesis and acts as a stabilizing agent, hence chosen for this study.

Several synthesis methods have been proposed to prepare Hydroxyapatite (HAp) such as; sol-gel, thermal hydrolysis, hydro thermal processing, chemical vapour deposition, thermal plasma approach and microwave synthesis method. Microwave synthesis method offers advantages than other techniques due to excellent compositional control, high homogeneity at the molecular level, lower crystallization temperature and feasibility of producing ultra fine nanorods [8,9].

The present work was an attempt to synthesize HAp and MOFE:HAp nanorods and to characterize their structural, morphological, thermal, optical and anti microbial properties.

2. Materials and methods:

2.1. Microwave assisted synthesis of HAp and MOFE:HAp

All the chemicals used for synthesizing HAp and MOFE:HAp nanorods were of analytical reagent grade (99% purity procured from Sigma - Aldrich, USA). The HAp and MOFE:HAp nanorods were prepared using calcium hydroxide [$Ca(OH)_2$], orthophosphoric acid [H_3PO_4], and sodium hydroxide [NaOH]. The 1 M of calcium hydroxide [$Ca(OH)_2$] was dissolved in 250 mL of de-ionized water and stirred for 10 min using magnetic stirrer. Similarly, 0.6 M of orthophosphoric acid [H_3PO_4] solution was also prepared and mixed with calcium hydroxide. The 0.8 M of NaOH was dissolved in 25 mL de-ionized water and the solution was added to the starting solution slowly from a burette held vertically with HAp until the pH value reached 12. Similarly, 50 g of *Moringa oleifera* flower [MOF] was cleaned and dried at room temperature. The prepared MOF was mixed with 250 mL de-ionized water and boiled for 2 h. Then the MOF extract was cooled at room temperature, filtered and stored at 4 °C for further use. MOFE solution was added to the above solution and stirring was continued for 1 h then kept at room temperature for 24 h to get a gelatinous precipitate. The obtained precipitate was dried for 10 min using 35 W domestic microwave oven and calcined at 100 °C furnace for one hour. Thus an obtained dried cake was crushed to obtain Hydroxyapatite (HAp) and *Moringa oleifera* flower extract capped Hydroxyapatite (MOFE:HAp) powders.

2.2. Characterization of HAp and MOFE:HAp

The dried samples were examined directly using XPERT-PRO, Burker AXS D8 Advance X-ray diffractometer. The structural parameters were calculated from the following equations [10]

$$\frac{1}{d^2} = \frac{4}{3}\left[\frac{h^2 + hk + k^2}{a^2}\right] + \frac{l^2}{c^2} \quad (1)$$

$$D = \frac{0.94\lambda}{\beta \cos\theta - 2\varepsilon \sin\theta} \quad (2)$$

$$\delta = \frac{1}{D^2} \quad (3)$$

$$\varepsilon = \frac{\lambda}{D\sin\theta} - \frac{\beta}{\tan\theta} \quad (4)$$

Where, d was the d-spacing, h,k,l were the miller indices, 'D' was the crystallite size, 'K' was the shape factor taken as 0.94, 'λ' was the wavelength of monochromatic X-Ray beam (nm), 'β' was the full width at half maximum for the diffraction peak under consideration (in radians), and 'θ' was the diffraction angle, 'δ' was the dislocation density and 'ε' was the micro strain. Transmission electron microscopy (TEM) using JEOL Model JSM – 6390 LV instrument for high resolution surface imaging and Philips CM20 super twin microscope respectively. Specimens for TEM were prepared by ultrasonic dispersion of some powder samples in ethanol and putting a droplet of the suspension on a copper microscope grid covered with carbon. IR spectra were taken with a Bruker IFS Table 88 spectrometer in the range 4000–400 cm^{-1}. The optical studies of the samples were done with a UV–Vis spectrophotometer (Model JASCO-V-570) in the range from 300 to 900 nm. An Ocean Optics (Dunedin, FL) setup was used to measure the diffuse reflectance spectra of the pallet samples. Eg was determined by applying the Kubelka-Munk or F(R) method. The K-M method was based on the following equation.

$$F(R) = \frac{(1-R)^2}{2R} \quad (5)$$

where, R was the reflectance; F(R) was proportional to the extinction coefficient (α). This equation was usually applied to highly light scattering materials and absorbing particles in a matrix. A modified K-M function could be obtained by multiplying the F(R) function by hν, using the corresponding coefficient (n) associated with an electronic transition as follows:

$$(F(R) * h\nu)^n \quad (6)$$

Where, n was an index, which assumed the values ½, 3/2, 2 or 3, depending on the nature of the electronic transition responsible for absorption mechanism of electron transition. The exponent n = 1/2, 3/2 for direct transition was allowed or forbidden and n = 2, 3 for allowed and forbidden indirect transition. The room temperature photoluminescence spectrum was performed on a spectrofluorimeter (Fluorolog Model FL3-11). TG/DTA measurements were carried out with the help of SII nanotechnology, TG/DTA 6200 at Nitrogen atmosphere. Samples weighing 20.0 ± 0.1 mg were heated in a ceramic sample boat up to 900 °C at 20 °C/min and in a stream (40 mL/min) of nitrogen gas.

2.3. Phytochemical analysis of MOFE and HAp formation

Phytochemical investigation of methanolic extract of *Moringa oleifera* flowers revealed the presence of flavonoid, tannin, saponin, steroid, phenol, carbohydrate and glycoside.

The formation mechanism of crystalline HAp nanorods was as follows. The polyphenolic hydroxyl groups of tannins (extract) produced a p-track conjugation effect and binded with Ca^{2+} to form Ca–tanninate complex by conjugation effect. During the addition of H_3PO_4 solution to the Ca– tanninate complex, the negative $PO4^{3-}$ group had ionic interaction with positive calcium ion for the formation of HAp–tanninate complex [11]. Finally, the resulting product was calcined at higher temperatures and the impure tanninate was eliminated to get pure HAp nanorods.

2.4. Antibacterial and antifungal activity of HAp and MOFE:HAp

The antibacterial and antifungal activity of HAp and MOFE:HAp was tested against the growth of bacteria and fungi by agar well diffusion method. The tested organisms were bacteria inoculated in Luria Bertani broth (pH 7.4) and fungi inoculated in potato dextrose broth for 18–24 h. The isolates were seeded on Luria Bertani agar and potato dextrose agar plates using sterilized cotton swabs. Agar surface was bored using sterilized gel borer to make wells (7 mm diameter). Different concentrations ranging from 25 to 75 μg/mL of HAp and MOFE:HAp and 100 μL of sterilized distilled water (negative control) were poured into separate wells. The plates were incubated at 37 °C for 24 h. Triplicate plates were maintained for each organism. The tested gram positive bacteria included; *Bacillus subtilis, Monococcus luteus and Staphylococcus aureus* while the tested gram negative bacteria included; *Klebsiella pneumoniae*, *Pseudomonas aeruginosa* and *Salmonella paratyphi.* Ciprofloxacin was used as a standard drug for the antibacterial studies. The antifugal studies were carried out on *Candida albicans*, *Aspergillus niger* and *Aspergillus fumigatus* using Fluconazole as standard antifungal drug.

Table 1
The phytochemical constituents of *Moringa oleifera* flowers.

Component	Test	Observation	Scoring
Alkaloid	Dragendorffs	Brownish-red colour	+
Tannins	Ferric chloride	Blue ink colour	+
Flavonoid	Pew's	Red colour	+
Saponin	Frothing	Persistence foam	+
Phenol	Buchard	Violet colour	+
Carbohydrate	Molisch's	Red colour	+
Glycosides	Salkowski's	Reddish brown	+

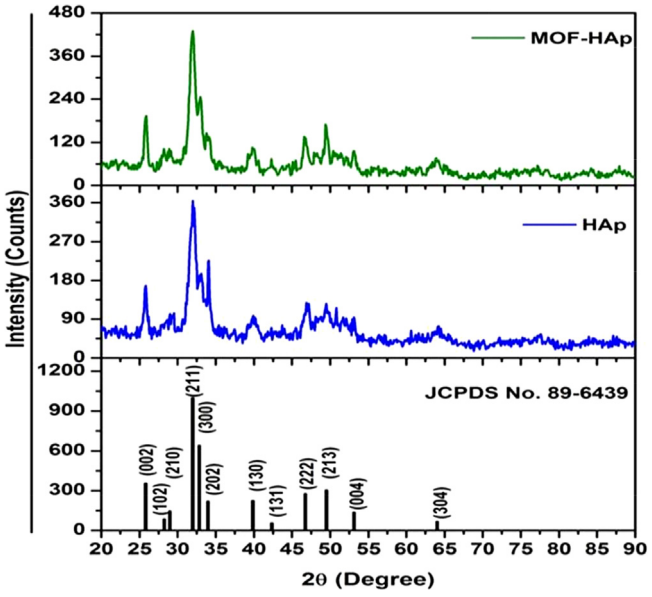

Fig. 1. Xray diffraction patterns of Hydroxyapatite and *Moringa oleifera* flower extract capped Hydroxyapatite nanorods.

2.5. Statistical analysis

The results were presented as mean + SD by using one-way analysis of variance (ANOVA) [12]. The level of significance was recognized at $P < .05$. Statistical analyses were performed by using Xlstatpro7.5.

3. results

3.1. X-ray diffraction analysis of HAp and MOFE:HAp nanorods

Moringa oleifera flower was rich in tannins as shown in (Table 1). Crystal structure and phase identification of the samples were analyzed from the X-ray diffraction pattern. The XRD pattern of the prepared samples of HAp and MOFE:HAp nanorods is shown in (Fig. 1). All samples confirmed the presence of hexagonal structure with preferred orientation along (2 1 1) plane. All other Bragg peaks with miller indices (00), (1 0 2), (2 1 0), (3 0 0), (2 0 2), (1 3 0), (1 3 1), (2 2 2), (2 1 3), (0 0 4) and (3 0 4) were associated with the hexagonal lattice of HAp and MOFE:HAp nanorods and it was in a good agreement with JCPDS card No. 89-6439. No other impurity peaks were detected. The MOFE:HAp samples increased with the increased intensity and decreased FWHM which confirmed improved crystallinity. The variation of lattice constants, crystallite size, dislocation density and micro strain of the HAp and MOFE:HAp nanorods were listed in (Table 2).

The average crystallite size was increased from 12.4 to 18.6 nm for HAp and MOFE:HAp nanorods. It might be assumed that the crystallite size was grown as a result of the interfacial reaction. The average crystallite size increased with decrease in lattice parameters. The lattice constants of HAp nanorods matched well with the standard values nearly. Both dislocation density and micro strain decreased for MOFE:HAp and improved the crystallinity of the sample.

3.2. Morphological analysis of HAp and MOFE:HAp nanorods

The surface morphology of HAp and MOFE:HAp nanorods is displayed in Fig. 2(a and b). Formation of agglomeration crystallites was

Table 2
Structural parameters of Hydroxyapatite and *Moringa oleifera* flower extract capped Hydroxyapatite nanorods.

Types of nanorods	2θ	d-spacing Å	FWHM	(hkl) Crystal System	Lattice constants Å		Crystallite size nm	Dislocation density (δ) 10^{14}lin/m^2	Micro strain (ε) 10^4 lin^{-2}m^{-4}
					a	c			
HAp	25.807	3.45232	0.5665	002			17.2	17.2	27.5
	28.2336	3.16088	1.0646	102			9.2	9.2	9.2
	28.9665	3.08255	1.0301	210			9.5	0.014	44.4
	31.9755	2.79901	0.9456	211			10.4	10.4	10.4
	32.8432	2.72702	0.8183	300			12.1	12.1	12.1
	33.9797	2.63837	1.3975	202	9.414	6.876	7.1	7.1	7.1
	39.8421	2.26264	0.6625	130			15.2	0.011	0.011
	42.3268	2.13539	0.9735	131			10.4	0.61	28.0
	46.7486	1.9432	0.7067	222			14.6	0.45	18.2
	49.508	1.84116	0.6128	213			17.0	0.45	14.8
	53.1146	1.72433	0.6283	004			16.9	16.9	14.0
	64.0235	1.45434	1.0945	304			10.2	9.46	19.5
	25.7505	3.45977	0.5522	002			17.6	0.421	26.9
	28.2000	3.16457	1.0089	102			9.7	0.013	44.7
	29.1915	3.05931	0.1435	210			68.4	2.802	6.1
	32.0482	2.79283	1.3117	211			7.5	0.023	50.8
	32.9604	2.71759	1.0827	300			9.1	0.015	40.7
MOFE:HAp	33.9775	2.63853	0.4532	202	9.405	6.867	21.9	0.273	16.5
	39.9394	2.25735	0.8836	130			11.4	0.010	27.0
	42.3846	2.13261	1.2082	131			8.4	0.018	34.7
	47.0413	1.93179	1.1047	222			9.3	0.014	28.2
	49.5028	1.84134	1.0741	213			9.7	0.013	25.9
	53.0159	1.72731	0.4201	004			25.2	0.205	9.3
	64.1739	1.4513	0.4382	304			25.6	0.0200	7.7

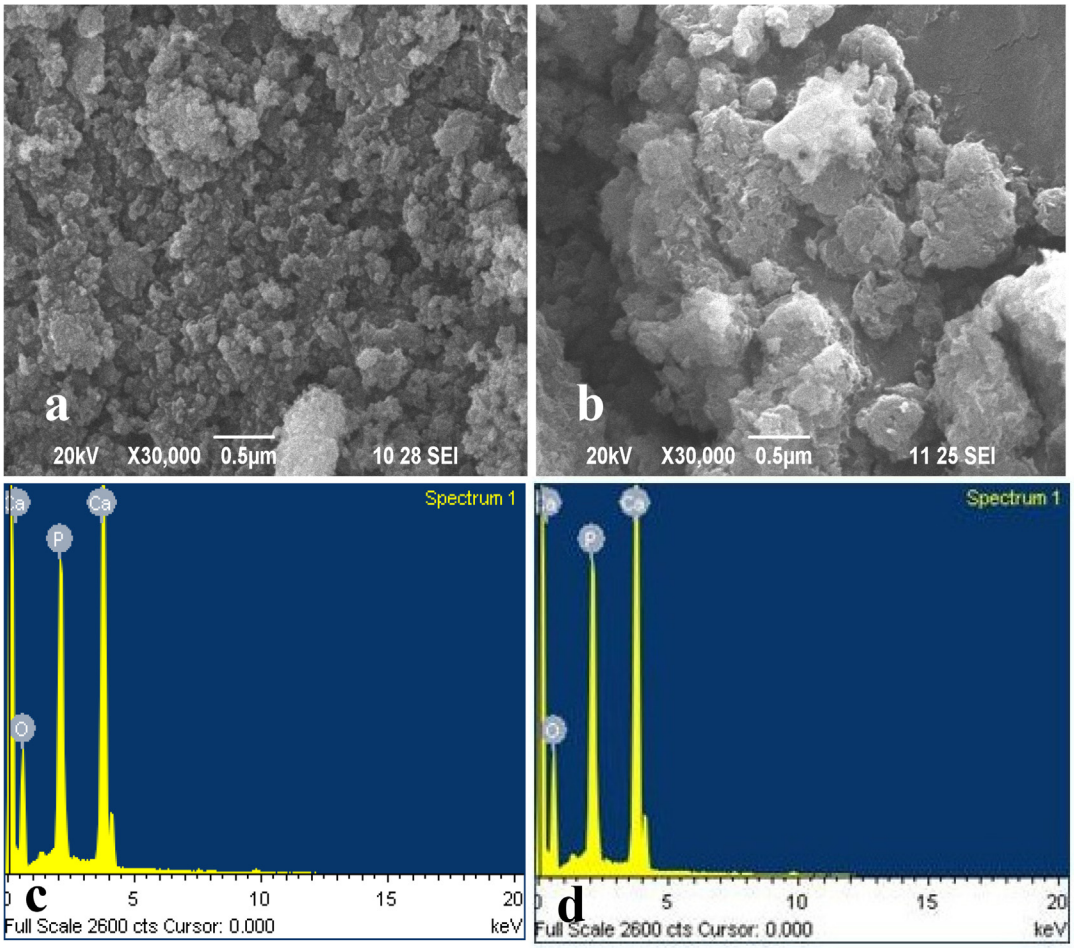

Fig. 2. (a). Scanning Electron Microscope images of Hydroxyapatite. (b). Scanning Electron Microscope images of *Moringa oleifera* flower extract capped Hydroxyapatite. (c). Energy Dispersive Analysis images of Hydroxyapatite. (d). Energy Dispersive Analysis images of *Moringa oleifera* flower extract capped Hydroxyapatite.

Table 3
Atomic percentage of Hydroxyapatite and *Moringa oleifera* flower extract capped Hydroxyapatite.

Types of nanorods	Elements			
	Ca (at.%)	P (at.%)	O (at.%)	Ca/P(at.%)
HAp	17.31	10.51	72.10	1.64
MOFE:HAp	17.90	9.84	72.25	1.81

attributed to uncontrolled coagulation. Small crystallites clinging together to form a large agglomerated structure with average grain size b ~18 nm was observed. In MOFE:HAp, a gradual increase in grain size 25 nm occurred due to a change of nucleation centers during incorporation of the MOFE into the host material. Further, MOFE:HAp nanorods showed that the entire region exhibited spherical shape with irregular uniform size. The MOFE modified similar surface morphology as HAp nanorods. Thus the SEM analysis resembled the XRD studies and showed large agglomerated grains with the size ranging from 50 to 80 nm.

3.3. Elemental analysis of HAp and MOFE:HAp nanorods

The energy dispersive analysis by X-ray (EDAX) of the HAp and MOFE:HAp nanorods is shown in Fig. 2(c and d). Only Ca, P and O peaks were observed indicating that HAp and MOFE:HAp product was obtained. The compositional analysis indicated the atomic ratio of Ca, P and O as 17.31 (calcium):, 10.51 (phosphorus), and 72.10 (oxygen) for HAp and 17.90 (calcium), 9.84 (phosphorus):, and 72.25 (oxygen) for MOFE:HAp. Elemental atomic percentages (%) of Ca, P and O elements in the samples are listed in (Table 3).

3.4. TEM analysis of HAp and MOFE:HAp nanorods

TEM images and the selected area electron diffraction (SAED) pattern of the Hap (Fig. 3a–c) and MOFE:HAp Fig. 3(d–f) nanorods were recorded. The crystal structure of the ellipsoidal HAp nanorods was basically monocrystalline with the rotation axis in accord with the c-axis of the hexagonal system. However, the surface structure was found rough and partly polycrystalline, the addition of MOFE was excessively increased it. This was due to the formation of dents, valleys, or crevices as a result of the locally clustered adsorption of the MOFE on the growing surfaces of the HAp nanorods. The distinct and good diffraction rings corresponding to the hexagonal phase were observed. The intensity of the diffraction rings indicated that the particles crystallized with a good crystalline nature and had a narrow size distribution. Each ring in the SAED pattern could be assigned to the prominent diffraction peaks of hexagonal HAp. TEM indicated the configuration of nanorod like structures on the samples with average diameter 41 nm.

3.5. Optical properties of HAp and MOFE:HAp nanorods

The FTIR spectrum of HAp and MOFE:HAp nanorods were recorded in the range of 400–4000 cm^{-1} as shown in (Fig. 4) and function groups

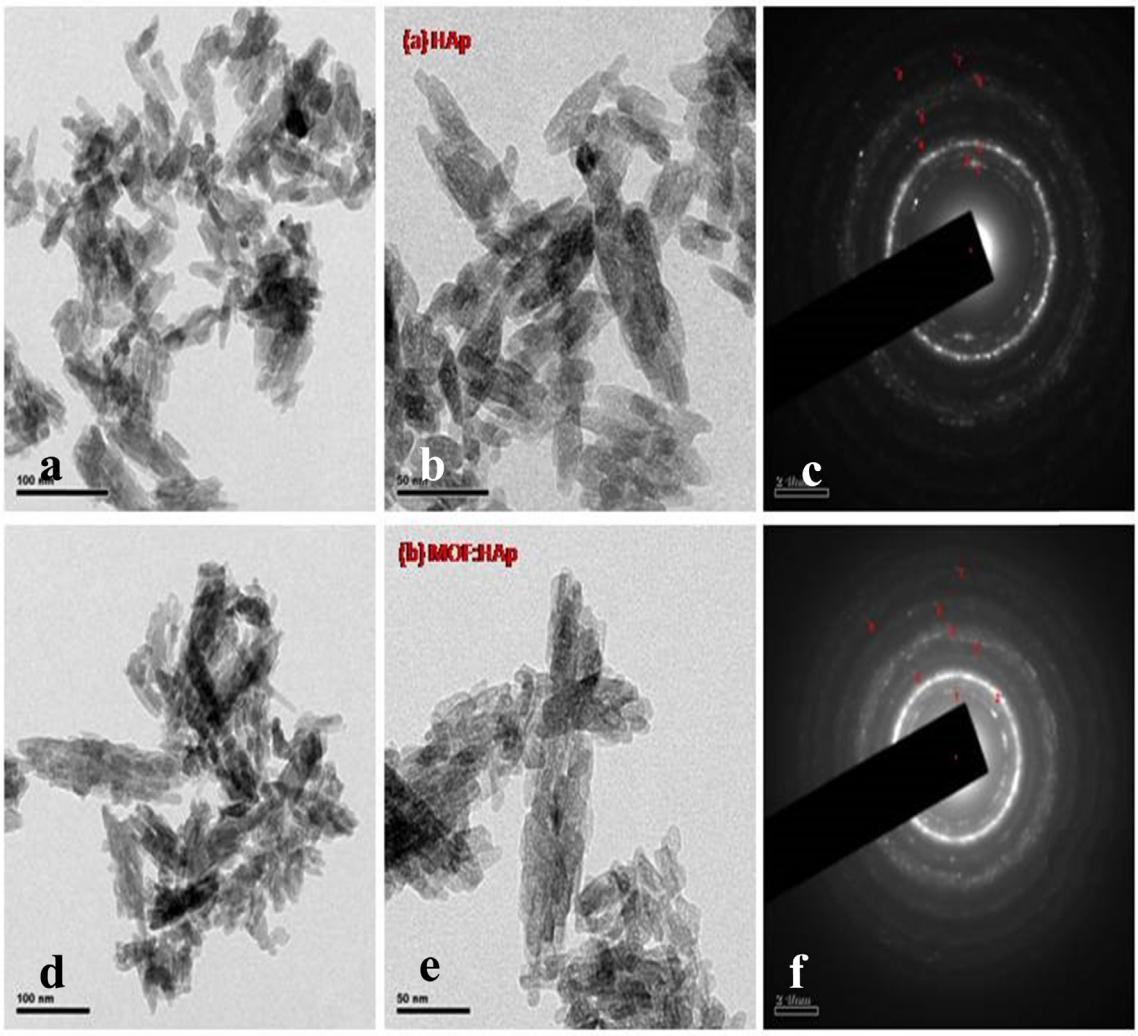

Fig. 3. (a and b) Transmission electron microscopy images of Hydroxyapatite, (c). Selective Area Electron Diffraction patterns of Hydroxyapatite, (d and e) Transmission electron microscopy images of *Moringa oleifera* flower extract capped Hydroxyapatite.(f) Selective Area Electron Diffraction patterns of *Moringa oleifera* flower extract capped Hydroxyapatite.

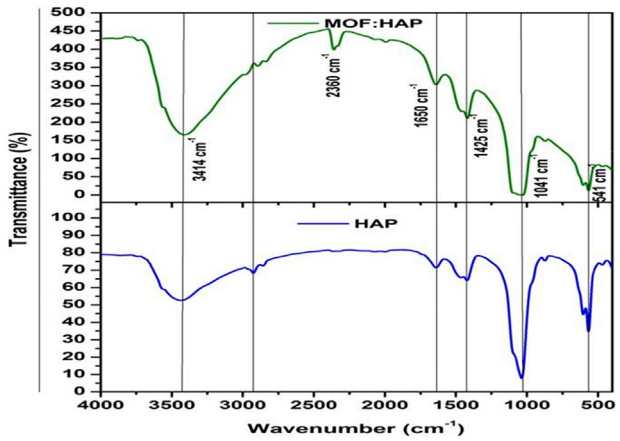

Fig. 4. Functional group interaction studies of Hydroxyapatite and *Moringa oleifera* flower extract capped Hydroxyapatite nanorods.

assignments are listed in (Table 4). The samples showed the vibrations of the various groups at different wave numbers of IR radiation. It was observed that the broad peaks at 3418.17 cm^{-1} and 1631.87 cm^{-1} due to the absorbed water, while the sharp peak at 3417.73 cm^{-1} due to the stretching vibrations of the lattice OH^- ions and the medium sharp peak at 649.35 cm^{-1} due to the OH^- deformation mode. The peak at 1631.87 cm^{-1} was assigned to bending mode of water. The intense broad peak between 900 cm^{-1} and 1100 cm^{-1} was assigned to stretching mode of PO_4^{3-}. The bending modes of PO_4^{3-} appeared at 620.65 cm^{-1} and 567 cm^{-1} as intense sharp peaks. The bands with shoulder at 962.54 cm^{-1} and 1013.99 cm^{-1} were assigned to the P-O stretching vibrations of the phosphate groups. The weak band at about 463.35 cm^{-1} corresponded to the Phosphate bending vibration. The peak at 874.66 cm^{-1} was caused by HPO_4^{2-} groups. The CO_3^- derived bands were observed at 1402 cm^{-1}–1460 cm^{-1}. It might be due to the absorption of an atmospheric carbon-di-oxide during the sample preparation. The weak peak at 3641.29 cm^{-1} corresponded to the vibrations of OH^- ions in the HAp lattice. This indicated that the samples are good in the assigned mode.

3.6. UV analysis of HAp and MOFE:HAp nanorods

The diffuse reflectance of HAp and MOFE:HAp nanorods is observed in (Fig. 5), the reflectance edge was shift to higher wavelength with addition of MOFE. The optical band gap of HAp and MOFE:HAp nanorods is shown in (Fig. 6). The band gap values for HAp and MOFE:HAp nanorods were in the range of 5.2–5.5 eV. The calculated band

Table 4
Function groups of Hydroxyapatite and *Moringa oleifera* flower extract capped Hydroxyapatite.

Types of nanorods	Functional groups (cm^{-1})						
	OH-Stretching mode (cm^{-1})	H_2O-Bending mode (cm^{-1})	PO_4^{3-}-Stretching mode (cm^{-1})	PO_4^{3-}-Bending mode (cm^{-1})	PO-Stretching mode (cm^{-1})	PO-Bending mode (cm^{-1})	HPO_4^{3-}(cm^{-1})
HAp	3417.73	1646	1039.41	567.4, 603.7	962.54	469.68	874.3
MOFE:HAp	3418.89	1631.89	1044.12	537.4, 620.6	924.10	463.35	875

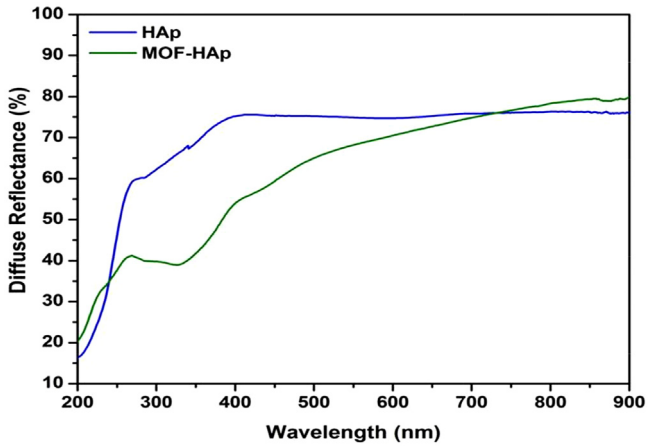

Fig. 5. Diffuse reflectance studies of Hydroxyapatite and *Moringa oleifera* flower extract capped Hydroxyapatite extract nanorods.

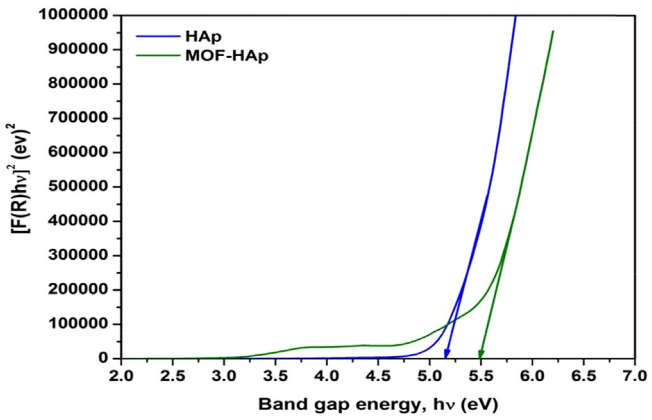

Fig. 6. Band gap energy of Hydroxyapatite and *Moringa oleifera* flower extract capped Hydroxyapatite nanorods.

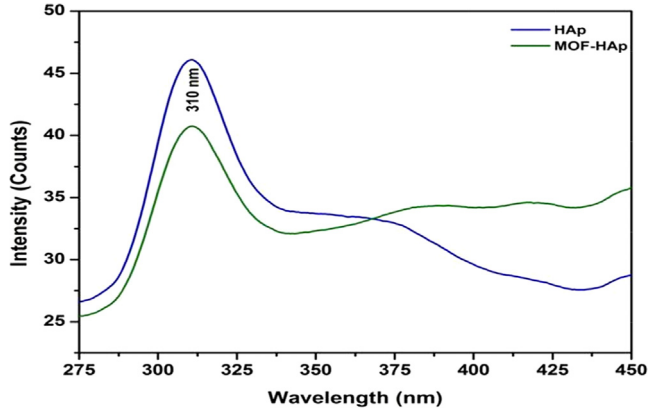

Fig. 7. Photo luminescence analysis studies of Hydroxyapatite and *Moringa oleifera* flower extract capped Hydroxyapatite nanorods.

gap of HAp using density functional theory has been reported in the range of 5.23 eV–5.40 eV. The experimental values have been reported from 3.45 eV to 5.78 eV.

3.7. PL analysis of HAp and MOFE:HAp nanorods

The photoluminescence of HAp and MOFE:HAp nanorods is shown in (Fig. 7). The samples were taken at room temperature employing the excitation wavelength of 275 nm. A broad visible emission band was around 310 nm for the HAp and MOFE:HAp nanorods. When HAp nanoparticles were exposed to UV light, these vacancies became liable to the trap holes produced by the UV exposure. The intensity of peaks decreased with addition of MOFE. The band gap of HAp and MOFE:HAp nanorods was found to be 5.2 eV and 5.5 eV respectively.

3.8. Thermal analysis of HAp and MOFE:HAp nanorods

The TGA/DTA analysis of HAp and MOFE:HAp nanorods is shown in (Fig. 8). The weight loss was observed in 4 stages. The first region corresponded to a 3.3% (HAp) and 1.4% (MOFE:HAp) weight loss that was observed in the range of 38 °C to 80 °C due to the presence of OH groups. The second region corresponded to a 16.7% (HAp) and 3.9% (MOFE:HAp) weight loss that was observed at the rang of 80–260 °C due to entrapped chemisorbed water, so amorphous phase changed to crystalline hexagonal phase. In HAp and MOFE:HAp, the third region corresponded to 7.3% (HAp) and 0.4% (MOFE:HAp) weight loss that was observed in the range 350–500 °C, due to decomposition of carbonates and other impurities. Thus, the MOFE:HAp samples had high thermal stability and phase stability. The differential thermal analysis (DTA) showed exothermic peaks in the temperature region of 220 and 278 for HAp and 220 and 268 for MOFE:HAp. The increase in thermal stability will improve the property of antibacterial at high temperature.

3.9. Antimicrobial activity

3.9.1. Antibacterial properties of HAp and MOFE:HAp nanorods

In the present study, The antibacterial activity of HAp and MOFE:HAp nanorods was investigated against both Gram positive and Gram negative bacteria by agar well diffusion method. The zone of inhibition was different among pathogens and the zone size increased when the concentration of HAp and MOFE:HAp nanorods was increased. Based on the data obtained, the zone of inhibition observed against gram positive bacteria *Bacillus subtilis, Monococcus luteus* and *Staphylococcus aureus* was 9 ± 1.03 mm,10 ± 1.1 mm and 11 ± 1.03 mm for HAp and 14 ± 1.05 mm,15 ± 0.9 mm and 13 ± 0.9 mm, respectively for MOFE:HAp. Similarly for gram negative bacteria *Klebsiella pneumoniae, Pseudomonas aeruginosa* and *Salmonella paratyphi* the zone of inhibition diameter values of the HAp were 9 ± 1.3 mm, 9 ± 1.2 mm, and 10 ± 1.0 mm and 10 ± 1.3 mm,10 ± 1.6 mm, and 12 ± 1.2 mm, respectively for MOFE:HAp. The zone of inhibition diameter values were measured for HAp and MOFE:HAp and tabulated in (Table 5) and in Fig. 9 (a1–a3). The bacterial inhibition was increased in MOFE:HAp nanorods when compared to HAp. The antibacterial effect of MOFE:HAp nanorods was superior on *Monococcus luteus* (15 ± 0.9 mm) of positive bacteria

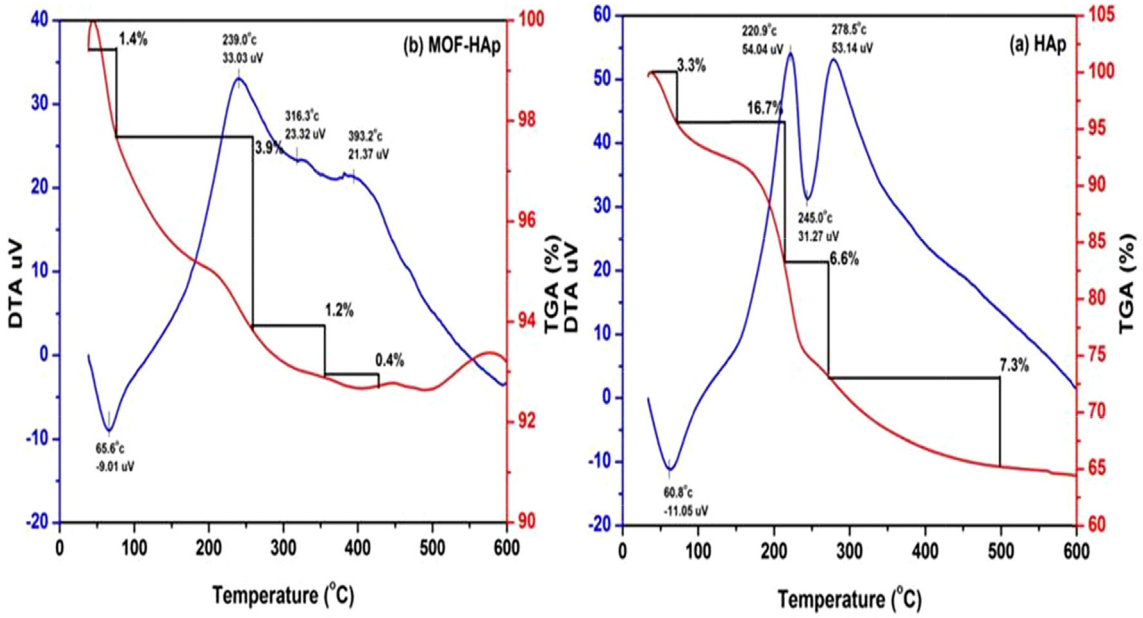

Fig. 8. Thermo gravimetric analysis of (a) Hydroxyapatite (b) *Moringa oleifera* flower extract capped Hydroxyapatite extract nanorods.

Table 5
Zone of inhibition values in millimeter (mm) level of the tested bacteria and fungi.

Types of nanorods	Bacteria								
	Gram positive bacteria			Gram negative bacteria			Fungi		
	Monococcus luteus	*Bacillus subtilis*	*Staphyllococcus aureus*	*Salmonella paratyphi*	*Klebsiella pneumoniae*	*Pseudomonas aeruginosa*	*Candida albicans*	*Aspergillus niger*	*Aspergillus fumigatus*
Standard	36 ± 1.02[a]	41 ± 0.9[a]	45 ± 1.0[a]	40 ± 1.0[a]	40 ± 1.8[a]	31 ± 1.8[a]	30 ± 0.9[a]	22 ± 0.8[a]	32 ± 1.0[a]
HAp	10 ± 1.1[b]	9 ± 1.03[b]	11 ± 1.03[b]	10 ± 1.0[b]	9 ± 1.3[b]	9 ± 1.2[b]	9 ± 1.2[b]	9 ± 1.1[b]	–
MOFE:HAp	15 ± 0.9[c]	14 ± 1.05[c]	13 ± 0.9[c]	12 ± 1.2[c]	10 ± 1.6[c]	10 ± 1.6[c]	16 ± 1.2[c]	10 ± 1.05[c]	15 ± 1.3[c]

Bars not labeled by the same letter represent statistical significance at $P \leq 0.05$ using ANOVA followed by Tukey's HSD test.

(Fig. 10). The antibacterial effect of MOFE:HAp nanorods was superior on *Salmonella paratyphi* (12 ± 1.2 mm) of gram negative bacteria (Fig. 9b1–b3). The zone of inhibition is displayed in (Fig. 11). Although the HAp nanorods were effective on gram positive and negative bacterium, MOFE:HAp nanorods had a significant higher antibacterial action than HAp nanorods.

3.9.2. Antifungal properties of HAp and MOF:HAp nanorods

Antifungal studies were performed using *Candida albicans, Aspergillus niger* and *Aspergillus fumigatus* and displayed in Fig. 9(c1–c3). The radial diameters of zone of inhibition observed against *Candida albicans* (9 ± 1.2 mm), *Aspergillus niger* (9 ± 1.1 mm) and no zone for *Aspergillus fumigatus* for HAp and 16 ± mm, 10 ± 1.05 mm, and 15 ± 1.3 mm, respectively for MOFE:HAp. The antifungal studies were performed with the standard *Fluconazole*. The antifungal studies showed a significant larger zone of inhibition for MOFE:HAp than HAp. MOFE:HAp nanorods inhibited all the three tested fungal strains whereas HAp was inactive against *Aspergillus fumigatus*. The zone of inhibition observed against the tested bacteria and fungi were displayed in the (Table 5) and (Fig. 12). MOFE:HAp nanorods had a significant higher antifungal activitiy than the HAp nanorods.

4. Discussion

The present study reported the green synthesis of Hydroxyapatite using *Moringa oleifera* flower extract. The result of the XRD pattern indicated the occurrence of sharp peaks due to the stabilization of the synthesized nanoparticles by the flower extract which acted as chelating agents, and thus confirmed the crystallization of the bioorganic phase occurring on the surface of Hydroxyapatite NPs [13]. The SEM image showed that HAp and MOFE-HAp were in nanorange. EDS analysis of HAp and MOFE HAp NPs revealed the presence of calcium, phosphorous and oxygen in proper proportion of 1.6 and 1.8, respectively. TEM analysis indicated the occurrence of hexagonal, triangular, and other non-spherical shapes during the green and chemical synthesis of pure and capped Hydroxyapatite nanoparticles. FTIR was used to identify the possible bio molecules responsible for the stabilization of the synthesized Hydroxyapatite NPs. The stability of *Moringa oleifera* capped Hydroxyapatite nanoparticle might be due to the free amino and carboxylic groups that have interacted with the calcium surface. The bonds of functional groups were derived from the amide bands that were derived from the proteins in the flower extract. These bonds were the capping ligands of the nanoparticle [14]. The calculated band gap of HAp using density functional theory has been reported in the range of 5.23 [15] to 5.40 eV [16]. Although, experimental values have been reported from 3.45 eV [17] to 5.78 eV [18]. These changes might be due to the shift in direct and indirect transition of electrons. The capping of MOFE had a minor variation on the wavelength of emission peaks. The luminescence intensity firstly improved and then decreased with the increasing of calcinations temperature. The highest value of luminescence intensity was observed at 400 °C while the lowest value was observed at 500 °C, which showed a temperature-dependent fluorescence quenching. The unpaired ground state electrons absorbed energy at 310 nm and moved to exited sate of HAp Nps. This band could

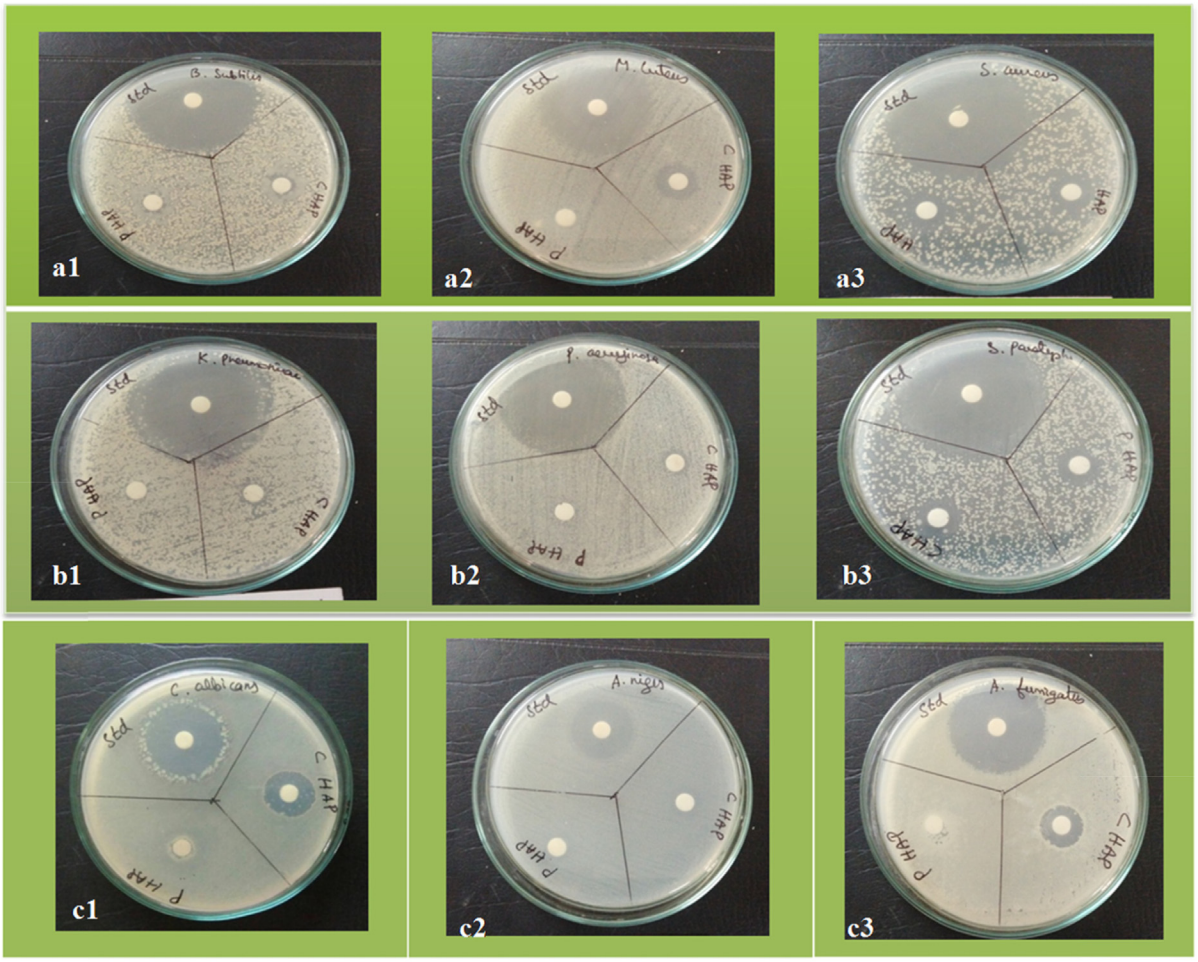

Fig. 9. Photographs of the antimicrobial activity of Hydroxyapatite and *Moringa oleifera* flower extract nanorods against Gram positive bacteria (a1–a3), Gram negative bacteria (b1–b3) and fungi (c1–c3).

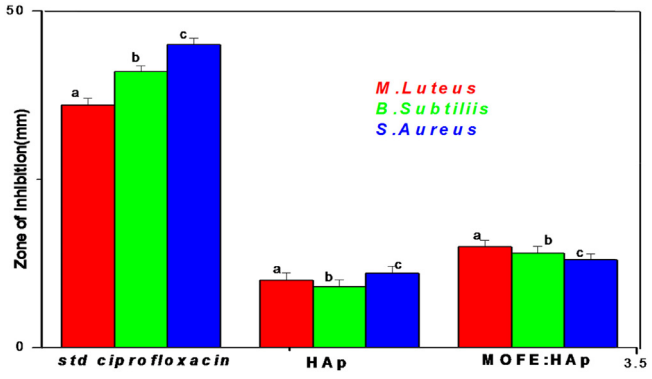

Fig. 10. Zone of inhibition graph against gram positive bacteria for Hydroxyapatite and *Moringa oleifera* flower extract capped Hydroxyapatite extract nanorods.

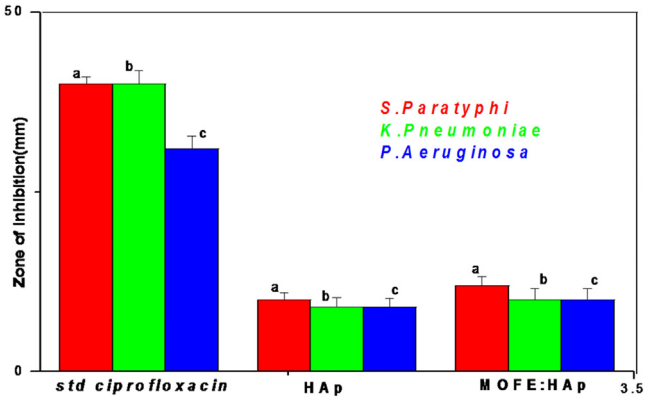

Fig. 11. Zone of inhibition graph against gram negative bacteria for Hydroxyapatite and *Moringa oleifera* flower extract capped Hydroxyapatite extract nanorods.

be attributed to the transition of electrons from low donor level of the oxygen vacancies in the valence band [19]. The luminescent efficiency depended upon the absorption efficiency of HAp at 310 nm in the excited state and produced a little non-radioactive transition. PL emission mainly resulted from the recombination of excited electron-hole pairs, and low emission intensity indicated a low intensity of recombination rate [20]. The synthesis method plays a vital role in decomposition temperature. The major mass loss was about 16.7% in HAp at 80–260 °C. This was due to endothermic peak credited to adsorbed water. This dominating mass loss was due to evaporation, desorption and burning of the residual OH solvent at 300–400 °C. The carbonate decomposition occurred from 400 to 500 °C. A slight decline in TGA curves showed the decomposition of Ca_{10} $(PO_4)_6$ in CaO and $Ca_3(PO_4)_2$ at 500 °C to 600 °C. This result matched well with the occurrence of CaO lines in the XRD patterns at 1000 °C. MOFE capping caused a minor influence on the thermal stability of HAp [21].

Staphylococcus aureus and *Pseudomonas aeruginosa* are the most

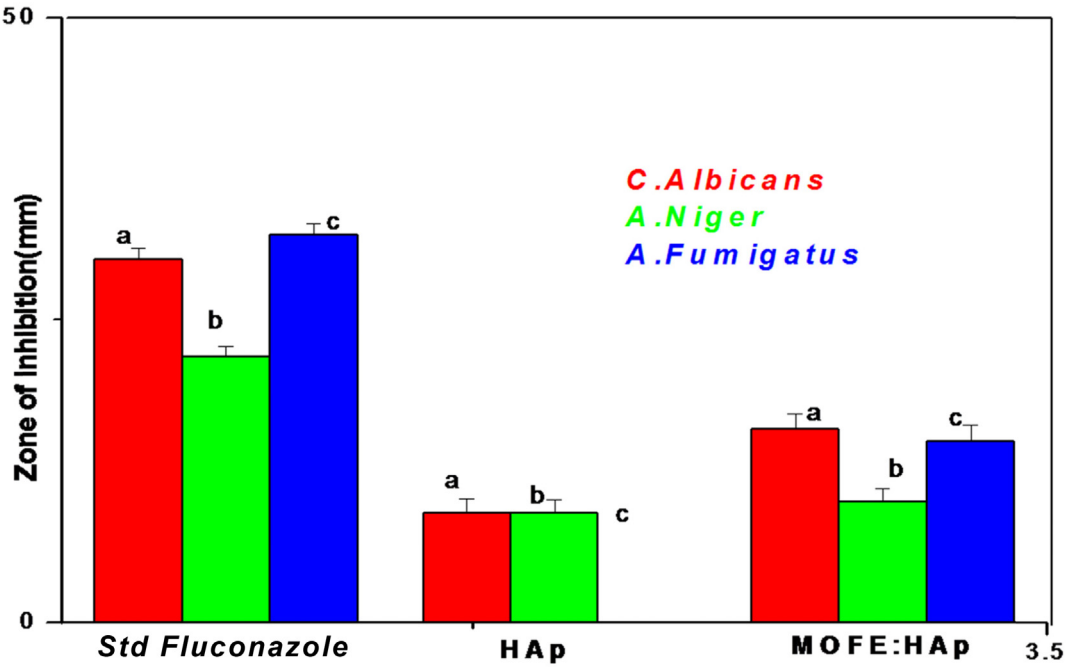

Fig. 12. Zone of inhibition graph against the tested fungi for Hydroxyapatite and *Moringa oleifera* flower extract capped Hydroxyapatite nanorods.

common pathogens causing diseases in bones and joints. *Ciprofloxacin* was the standard used for the antibacterial studies. The use of ciprofloxacin in the treatment of bone infections reduces the duration of therapy and improves the efficiency of bone tissue. Doses of *Ciprofloxacin* contribute to the decrease of development of resistant strains [22]. In both the samples, the standard value remained high since the dose of the antibiotic must be large to ensure its suitable concentration around the inserted implants [23,24]. There are three mechanisms explaining the antimicrobial activity. Initially, the ions break into the bacterial cell and affect the production of intracellular ATP and disturb the process of DNA reproduction. Secondly, it leads to ion growth in bacterial cell membrane and causes disturbance in the release of proteins and polysaccharides. When proton transportation through the cell membrane is prevented it leads to cell membrane destruction and bacterial cell death. Finally, the ion stimulation of reactive oxygen species (ROSs) that causing death of the bacterial cell. The antimicrobial mechanism of Hydroxyapatite nanorods was recognized by their contact with the strongly electronegative microbial surface [25]. NPs are very small; they can easily go through the tissues and cells of organisms, gather, and transfer to high-level organisms by food and soil chain. Therefor, HAp nanoparticles had and advanced antibacterial efficiency against *Escherichia coli* [25]. The possible mechanism for their antibacterial effect was based on the rough surface ordering of HAp due to surface defects and aggregates which contributed to the mechanical damage to the cell membrane of the bacteria [26]. The capping of MOFE improved the antibacterial and antifungal efficiency of Hydroxyapatite nanorods.

5. Conclusions

The present study concluded that *Moringa oleifera* flower extract Hydroxyapatite nanorods MOFE:HAp can be rapidly green synthesized using *Moringa oleifera* flower extract. These nanorods were inexpensive, non-toxic and ecofriendly with average size of 41 nm exhibiting rod structures. The green synthesized MOFE:HAp nanorods had greater antibacterial activity against Gram positive than Gram negative bacteria. Moreover, MOFE:HAp nanorods had antifungal activity against common pathogenic fungi. The outcomes of this study illustrated a broad range of notable applications of MOFE:HAp nanorods in biomedical fields in the future.

Acknowledgment

The corresponding author V.K thanks the Department of Physics, Navarasam Arts & Science college for Women, Erode for providing laboratory facilities and Prof. B. Vaseeharan and Mr. S. Vijayakumar for their help in manuscript preparation.

Competing interests

All authors declare no conflict of interests.

References

[1] Kumar GS, Rajendran S, Karthi S, Govindan R, Girija EK, Karunakaran G, et al. Green synthesis and antibacterial activity of hydroxyapatite nanorods for orthopedic applications. MRS Commun 2017;17(7):183–8.
[2] Gayathri B, Muthukumarasamy N, Velauthapillai D, Santhosh SB. Magnesium incorporated hydroxyapatite nanoparticles: preparation, characterization, antibacterial and larvicidal activity. Arabian J Chem 2016;11:645–54.
[3] Sahoo SK, Parveen S, Panda JJ. The present and future of nanotechnology in human health care. Nanomedicine 2007;1:20–31.
[4] Barry NP, Sadler PJ. Challenges for metals in medicine: how nanotechnology may help to shape the future. ACS Nano 2013;7:5654–9.
[5] Faghihi-Sani MA, Arbabi A, Mehdinezhad-Roshan A. Crystallization of hydroxyapatite during hydrothermal treatment on amorphous calcium phosphate layer coated by PEO technique. Ceram Int 2013;39:1793–8.
[6] Fu G, Vary PS, Lin CT. Anatase TiO_2 nanocomposites for antimicrobial coatings. J Phys Chem B 2005;109:8889–98.
[7] Remu A, Kingsley EI, Talha BK, Akeem AO, Ibrahim RA, Jimoh AG, et al. Methanolic leaf extract of *Moringa oleifera* improves the survivability rate, weight gain and histopathological changes of Wister rats infected with *Trypanosoma brucei*. Int J Vet Sci Med 2018;6:39–44.
[8] Manju S, Malaikozhundan B, Vijayakumar S, Shanthi S, Jaishabanu A, Ekambaram P, et al. Antibacterial, antibiofilm and cytotoxic effects of *Nigella sativa* essential oil coated gold nanoparticles. Microb Pathog 2016;91:129–35.
[9] Mariappan R, Ponnuswamy V, Suresh P. Effect of doping concentration on the structural and optical properties of pure and tin doped zinc oxide thin films by nebulizer spray pyrolysis (NSP) technique. Superlattices Microstruct 2012;52:500–13.
[10] Slepko A, Demkov AA. First-principles study of the biomineral hydroxyapatite. Phys Rev B 2011;84:134108.
[11] Sundrarajan M, Jegatheeswaran S, Selvam S, Sanjeevi N, Balaji M. The ionic liquid assisted green synthesis of hydroxyapatite nanoplates by *Moringa oleifera* flower extract: a biomimetic approach. Mater Des 2015;88:1183–90.

[12] Mann HB, Whitney DR. On a test of whether one of two random variables is stochastically larger than the other. Ann Math Stat 1947;1:50–60.
[13] Costescu A, Pasuk I, Ungureanu F, Dinischiotu A, Costache M, Huneau F, et al. Physico- chemical properties of Nano-sized Hexagonal Hydroxyapatite powder synthesized by sol- gel. Dig J Nanomater Biostruct 2010;5:989–1000.
[14] Thaya R, Malaikozhundan B, Vijayakumar S, Sivakamavalli J, Jeyasekar R, Shanthi S, et al. Chitosan coated Ag/ZnO nanocomposite and their antibiofilm, antifungal and cytotoxic effects on murine macrophages. Microb Pathog 2016;100:124–32.
[15] Calderin L, Stott MJ, Rubio A. Electronic and crystallographic structure of apatites. Phys Rev B 2003;67:134106.
[16] Bystrov VS, Piccirillo C, Tobaldi DM, Castro PM, Coutinho J, Kopyl S, et al. Oxygen vacancies, the optical band gap (Eg) and photocatalysis of hydroxyapatite: comparing modelling with measured data. Appl Catal B 2016;5:100–7.
[17] Tsukada M, Wakamura M, Yoshida N, Watanabe T. Band gap and photocatalytic properties of Ti-substituted hydroxyapatite: comparison with anatase-TiO2. J. Mol. Catal. A: Chem 2011;338:18–23.
[18] Mariappan R, Ragavendar M, Ponnuswamy V. Growth and characterization of chemical bath deposited Cd1 − xZnxS thin films. J Alloy Compd 2011;509:7337–43.
[19] Fan X, Wan J, Liu E, Sun L, Hu Y, Li H, et al. High-efficiency photoelectrocatalytic hydrogen generation enabled by Ag deposited and Ce doped TiO2 nanotube arrays. Ceram Int 2015;41(3):5107–16.
[20] Kalaiselvi V, Mathammal R, Anitha P. Sol-gel mediated synthesis of pure hydroxyapatite at different temperatures and silver substituted hydroxyapatite for biomedical applications. J Biotechnol Biomater 2017;7:1–6.
[21] Kolmas J, Groszyk E, Kwiatkowska-Rózycka D. Substituted hydroxyapatites with antibacterial properties. BioMed Res Int 2014. 178123.
[22] Pandya Haresh M, Anitha P, Mathammal R, Kalaiselvi V. Incorporation and in vitro application of hydroxyapatite with silver and titanium dopants synthesized by wet chemical method. J Environ Nanotechnol 2017;6:42–6.
[23] Kalaiselvi V, Mathammal R, Anitha P. Synthesis and characterization of hydroxyapatite nanoparticles using wet chemical method. Int J Adv Sci Eng 2017;4:71–574.
[24] Yin H, Li Y, Bai J, Ma M, Liu J. Effect of calcinations temperature on the luminescence intensity and fluorescent lifetime of Tb3 + -doped Hydroxyapatite (Tb-HA) nanocrystallines. J Materiomics 2017;3:144–9.
[25] Ragab HS, Ibrahim FA, Abdallah F, Al-Ghamdi Attieh A. Synthesis and in vitro antibacterial properties of hydroxyapatite nanoparticles. Int J Pharm Biol Sci 2014;9(1):77–85.
[26] Vijayakumar S, Malaikozhundan B, Shanthi S, Vaseeharan B, Thajuddin N. Control of biofilm forming clinically important bacteria by green synthesized ZnO nanoparticles and its ecotoxicity on *Ceriodaphnia cornuta*. Microb Pathog 2017;107:88–97.